



Cite this: *Phys. Chem. Chem. Phys.*,
2017, **19**, 29237

Received 11th September 2017,
Accepted 5th October 2017

DOI: 10.1039/c7cp06180c

rsc.li/pccp

Phonon-mediated superconductivity in Mg intercalated bilayer borophenes

Ji-Hai Liao,^a Yin-Chang Zhao,^{ib}*^b Yu-Jun Zhao,^{ac} Hu Xu^{ib}^d and Xiao-Bao Yang^{ib}*^{ac}

Using first-principles calculations, we investigate the structural, electronic and superconducting properties of Mg intercalated bilayer borophenes B_xMgB_x ($x = 2-5$). Remarkably, B_2MgB_2 and B_4MgB_4 are predicted to exhibit good phonon-mediated superconductivity with a high transition temperature (T_c) of 23.2 K and 13.3 K, respectively, while B_4MgB_4 is confirmed to be more practical based on the analyses of its stability. The densities of states of in-plane orbitals at the Fermi level are found to be dominant at the superconducting transition temperature in Mg intercalated bilayer borophenes, providing an effective avenue to explore Mg–B systems with high T_c s.

Introduction

Two-dimensional (2D) materials including graphene,¹ silicene,²⁻⁴ phosphorene,^{5,6} and h-BN⁷⁻⁹ have attracted tremendous interest due to their novel properties. Theoretical studies have suggested a set of freestanding borophenes by introducing hexagonal vacancies in the triangular lattice,¹⁰⁻¹⁵ where the hexagonal vacancy density (η) and the coordination number (CN) of boron atoms are used for the description and classification of borophenes.¹¹ Experimentally, borophenes of a striped phase (δ_6 ¹⁶ and β_{12} ¹⁷) and a homogeneous phase (χ_3 ¹⁷) have been successfully synthesized on a Ag(111) surface using a B atomic source, as confirmed by first-principles simulations.^{18,19} During the nucleation and growth on the Ag(111) surface,²⁰ the β_{12} sheet with 1/6 vacancies is energetically preferable, whose computed band structures agree with the observed angle-resolved photoelectron spectrum,²¹ with the simulated STM image in better agreement with the experimental observation.²² Due to their structural diversity, borophenes have been supposed to possess potential applications in catalysis,²³ Li-ion batteries,²⁴⁻²⁶ electronic devices,²⁷⁻³² and superconductors.³³⁻³⁸

Due to the vanished density of states at the Fermi level, metal adatom doping is necessary to induce superconductivity in a graphene sheet.^{39,40} The superconducting transition temperatures (T_c s) were estimated to be 8.1 K and 1.4 K for monolayer

LiC₆ and CaC₆, respectively, while they were 0.9 K and 11.5 K for graphite intercalated compounds LiC₆ and CaC₆.^{41,42} In a recent experiment, Li-intercalated bilayer graphene (C₆LiC₆) showed no sign of superconductivity down to 0.8 K, while superconductivity was observed at 2 K in Ca-intercalated bilayer graphene (C₆CaC₆).⁴³ Different from graphene, borophenes are mostly metallic, and the conventional BCS superconductivity in borophenes³³⁻³⁶ and 2D boron allotropes⁴⁴ is ubiquitous. In the bulk MgB₂ with a high T_c of 39 K, phonon-mediated superconductivity stems from the boron layers, owing to the in-plane stretching vibrational modes of boron.⁴⁵⁻⁴⁹ The T_c s in other bulk Mg–B systems, e.g. MgB₃, Mg₃B₁₀, and MgB₄, were estimated to be below 3 K,⁵⁰ and the T_c in Mg intercalated bilayer kagome borophene (B₃MgB₃–kagome) was predicted to be 4.7 K.⁵¹

In this paper, we have investigated Mg intercalated bilayer borophenes with $\eta = 1/3, 1/4, 1/5$, and $1/6$, focusing on their structural stabilities, electron–phonon coupling (EPC) properties and possible superconductivity. The projected electronic density of states (EDOS) and Eliashberg function are calculated to demonstrate the superconducting mechanism in these structures, as well as the orbital-resolved and phonon-perturbed band structures and the corresponding vibrational patterns. We predict that a metastable sandwich structure of B₂MgB₂ exhibits superconductivity with the highest T_c , where the B atoms form a hexagonal lattice with a triangular Mg sheet. To balance the structural stability and superconducting properties, B₄MgB₄ will be more practical according to the formation enthalpy *versus* T_c characteristics.

Methods

Our calculations were performed based on density functional theory (DFT) implemented in the QUANTUM-ESPRESSO package.⁵²

^a Department of Physics, South China University of Technology, Guangzhou 510640, P. R. China. E-mail: scxyang@scut.edu.cn

^b Department of Physics, Yantai University, Yantai 264005, P. R. China. E-mail: y.zhao@ytu.edu.cn

^c Key Laboratory of Advanced Energy Storage Materials of Guangdong Province, P. R. China

^d Department of Physics, South University of Science and Technology of China, Shenzhen 518055, P. R. China

The LDA norm-conserving scheme (von-Barth–Car type) was used to generate pseudopotentials for B and Mg. The plane-wave cutoff energy was set to 100 Ry. A vacuum region of 15 Å was adopted to avoid the interaction of the periodic images. All the structures were fully relaxed until the Hellmann–Feynman force on each atom was less than 10^{-5} Ry per Bohr. A Methfessel–Paxton⁵³ smearing width of 0.02 Ry was used for the corresponding electronic self-consistent cycles. For calculations of electronic properties, $16 \times 16 \times 1$ ($16 \times 12 \times 1$) Monkhorst–Pack⁵⁴ k meshes were used for B_2MgB_2 , B_3MgB_3 , and B_4MgB_4 (B_5MgB_5). The phonon frequencies and EPC parameter λ were calculated with $8 \times 8 \times 1$ and $8 \times 6 \times 1$ phonon wave-vector meshes and $64 \times 64 \times 1$ and $64 \times 48 \times 1$ denser k meshes, respectively. To estimate T_c , the McMillan–Allen–Dynes formula⁵⁵ was used with a retarded Coulomb pseudopotential μ^* of 0.1.

Results and discussion

The structures of Mg intercalated bilayer borophenes considered in this paper are schematically shown in Fig. 1(a). 2D B_2MgB_2 is constructed from layered bulk MgB_2 , and the B_2 (δ_3) sheet with $\eta = 1/3$ is a hexagonal lattice. There are two typical configurations for borophenes with $\eta = 1/4$, named δ_4 ¹¹ and kagome (see the inset of Fig. 1(b)).⁵¹ The Mg intercalated bilayer kagome borophene (B_3MgB_3 -kagome) was predicted to be a superconductor with $T_c = 4.7$ K.⁵¹ Energetically, the Mg intercalated bilayer δ_4 borophene (B_3MgB_3) shown in Fig. 1(a) with a calculated T_c of 6.0 K (see Fig. 1(b)) is more stable than the B_3MgB_3 -kagome by 0.075 Ry per cell (1.02 eV per cell). The Mg intercalated bilayer χ_3 borophene (B_4MgB_4), whose λ is estimated to be 0.64 (see Table 1), has a little higher T_c than the monolayer χ_3 sheet. Surprisingly, the superconductivity vanishes in the Mg intercalated bilayer β_{12} borophene (B_5MgB_5), while the β_{12} borophene's T_c was estimated to be 13.8 K.³⁴

In order to study the relative structural stability of the Mg intercalated bilayer borophenes (B_xMgB_x), we have calculated the formation enthalpy $\Delta H(x)$ as⁵⁶

$$\Delta H(x) = E_x - yE_1 - (1 - y)E_0,$$

where E_x , E_1 , and E_0 are the normalized total energies of B_xMgB_x , bulk Mg, and the α sheet, respectively, and $y = 1/(1 + 2x)$. As shown in Fig. 1(b), the formation enthalpies of B_3MgB_3 , B_4MgB_4 , and B_5MgB_5 are all negative, indicating the relative stability of these 2D structures. B_2MgB_2 and B_3MgB_3 -kagome⁵¹ should be less stable because of the positive formation enthalpy.

Experimentally, the layered bulk MgB_2 is found to be superconducting with a T_c of 39 K. Our calculated T_c for MgB_2 is 24.8 K, which is in agreement with previous computational results.^{50,57} Note that the calculated T_c is 23.2 K for 2D B_2MgB_2 from the layered bulk MgB_2 , which is the highest T_c in the low-dimensional Mg–B system. For comparison, we consider the artificial layered bulk MgB_x based on the sandwich structure B_xMgB_x , including the layered bulk MgB_3 , MgB_4 , and MgB_5 . Our calculations indicate that MgB_3 and MgB_4 are dynamically stable, while the dynamical stability of the layered bulk MgB_5 is

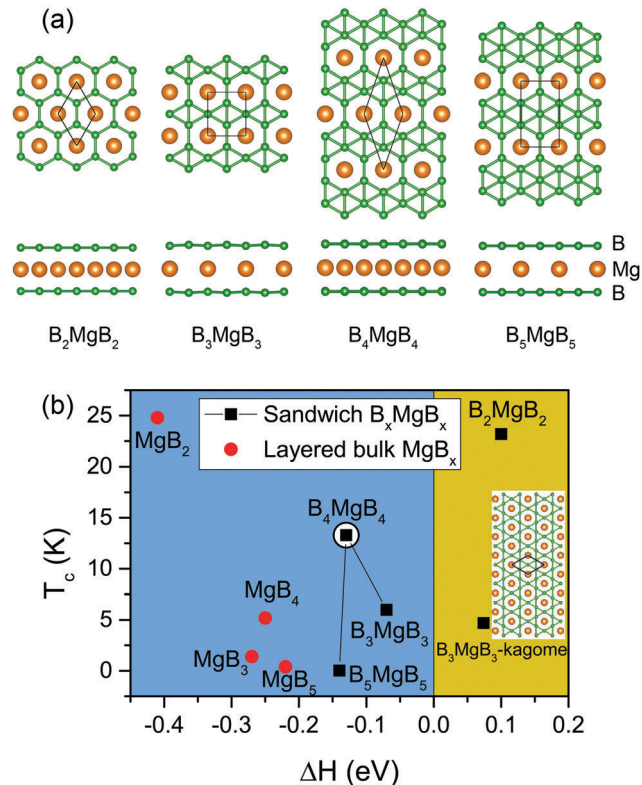


Fig. 1 (a) The 2D sandwich structures of B_2MgB_2 , B_3MgB_3 , B_4MgB_4 , and B_5MgB_5 with the top view and the side view. The big orange and small green balls represent Mg and B, respectively. The segments enclosed by solid black lines denote the unit cells for each structure. (b) Calculated T_c as a function of formation enthalpy. The inset in (b) is the top view of the configuration of Mg intercalated bilayer kagome borophene.⁵¹

Table 1 Calculated values of N_F , λ , ω_{\log} , and T_c for B_xMgB_x ($x = 2-5$). For comparison, the corresponding values of monolayer B_x sheets (δ_3 , δ_4 , χ_3 , and β_{12}) and layered bulk MgB_x are also listed. T_c was calculated using the McMillan–Allen–Dynes formula⁵⁵ with $\mu^* = 0.1$

	N_F (in-plane + p_z) (states per eV per cell)	λ	ω_{\log} (cm^{-1})	$T_c^{\mu^*=0.1}$ (K)
B_2MgB_2	0.97 (0.67 + 0.30)	0.71	652.3	23.2
B_3MgB_3	0.73 (0.41 + 0.32)	0.49	554.2	6.0
B_4MgB_4	0.96 (0.51 + 0.45)	0.64	491.6	13.3
B_5MgB_5	0.57 (0.07 + 0.50)	0.25	728.5	0.03
B_2 (δ_3 sheet)	0.67 (0.49 + 0.18)	1.13	384.7	31.9 ³⁴
B_3 (δ_4 sheet)	0.44 (0.35 + 0.09)	0.52	424.8	5.9
B_4 (χ_3 sheet)	0.59 (0.13 + 0.46)	0.67	388.4	12.1 ³⁴
B_5 (β_{12} sheet)	0.67 (0.31 + 0.36)	0.82	280.2	13.8 ³⁴
MgB_2	0.37 (0.20 + 0.17)	0.69	740.3	24.8
MgB_3	0.26 (0.09 + 0.17)	0.36	665.0	1.4
MgB_4	0.32 (0.14 + 0.18)	0.49	457.3	5.2
MgB_5	0.27 (0.04 + 0.23)	0.31	475.9	0.4

poor due to the presence of imaginary phonon frequencies in the Brillouin zone. Among these bulk structures, the densities of states of the in-plane orbitals at the Fermi level are dominant at the superconducting T_c , as shown in Table 1. Interestingly, for the Mg intercalated bilayer borophenes, it is also found that

T_c decreases with decreasing in-plane EDOS at the Fermi level, rather than the total EDOS. This finding provides an effective avenue to explore Mg–B systems with high T_c s.

In a previous theoretical study, the T_c of pristine borophenes decreases as the stabilities increases, where the B_2 (δ_3), B_3 (δ_4), B_4 (χ_3), and B_5 (β_{12}) sheets with higher T_c s are less stable than the α sheet.³⁴ The strain from the substrate and carrier doping also modulates T_c .³⁷ Note that the negative formation enthalpies of B_3MgB_3 , B_4MgB_4 , and B_5MgB_5 show that the structural stabilities of the Mg intercalated bilayer borophenes can be greatly enhanced. Moreover, the Mg intercalated borophenes

also show the possible low-dimensional boron–magnesium configurations and their changed superconducting properties due to their reduced dimensions compared with their bulk counterparts.

To balance the structural stability and superconducting properties, we show the calculated T_c s of these Mg–B structures as a function of formation enthalpy in Fig. 1(b). The formation enthalpies of bulk MgB_x are all lower than those of sandwich structures. Among magnesium borides, except for bulk MgB_2 , the other superconducting ones in previous theoretical studies had T_c s below 3 K;⁵⁰ herein, the layered MgB_4 has a calculated

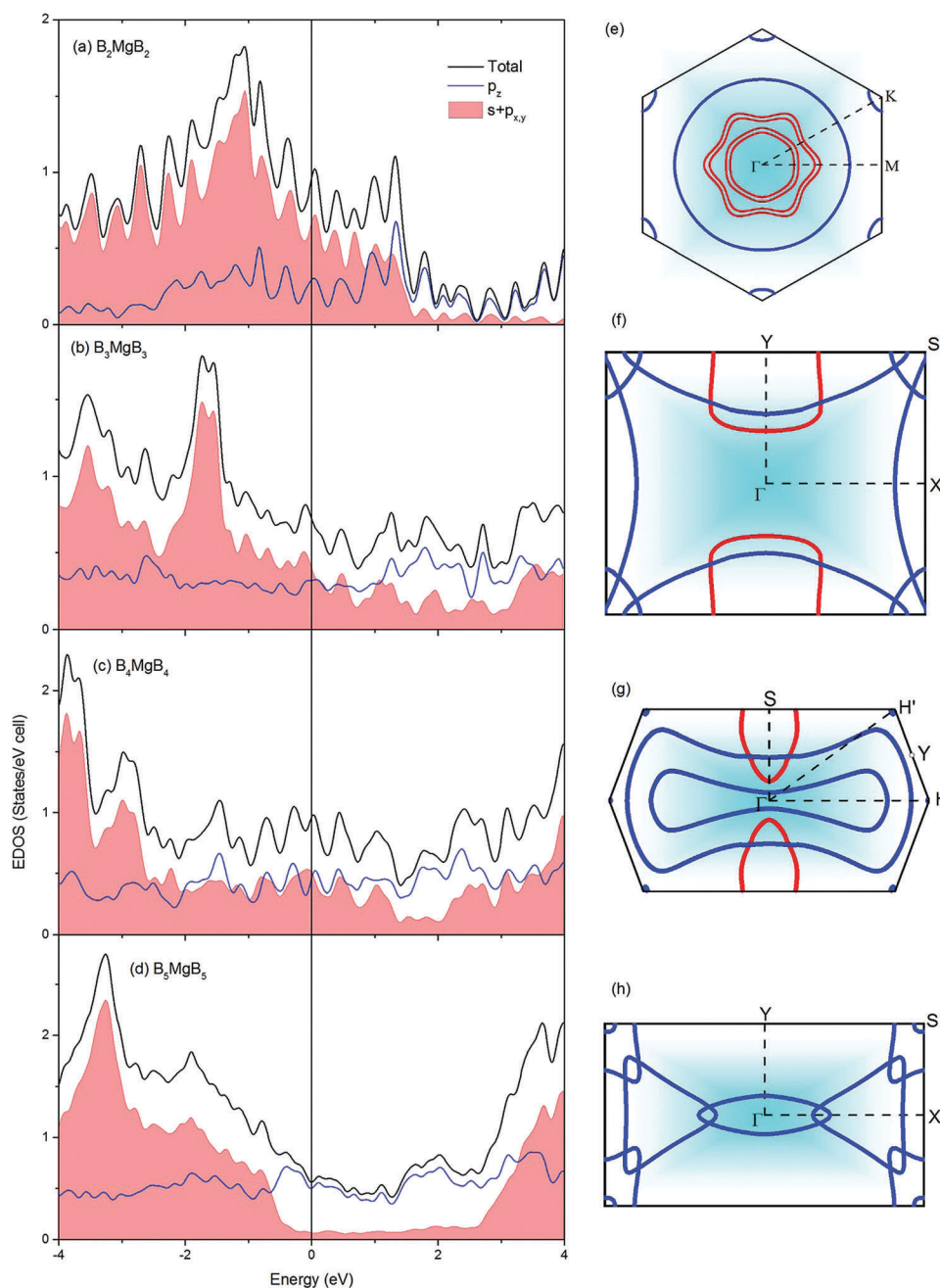


Fig. 2 The projected EDOS of (a) B_2MgB_2 , (b) B_3MgB_3 , (c) B_4MgB_4 , and (d) B_5MgB_5 , and the Fermi surfaces of (e) B_2MgB_2 , (f) B_3MgB_3 , (g) B_4MgB_4 , and (h) B_5MgB_5 . The Fermi level is set to zero, marked by the solid black line.

T_c of 5.2 K. MgB_2 is the most stable with the highest T_c . Of the sandwich structures, B_2MgB_2 possesses the highest T_c but with the poorest structural stability, B_3MgB_3 and B_5MgB_5 are more stable compared with B_2MgB_2 , while the corresponding T_c s are much lower. Split the difference, B_4MgB_4 has a high calculated T_c of 13.3 K combined with a relatively good structural stability, which will be more practical in superconducting applications.

According to conventional BCS theory,⁵⁸ the phonon-mediated superconductivity depends on the characteristic phonon frequency ω_0 and the EPC parameter λ ,

$$\lambda = N_F V_{\text{ep}},$$

where N_F is the EDOS at the Fermi level and V_{ep} is the effective pairing attractive potential.⁴⁴ Compared with the χ_3 (B_4) sheet, the N_F of B_4MgB_4 is increased by $\sim 60\%$, which comes from the in-plane orbitals ($s + p_x + p_y$). However, the N_F of B_5MgB_5 is reduced by $\sim 15\%$ than that of the β_{12} (B_5) sheet, and the contribution of the in-plane orbitals is decreased by $\sim 80\%$.

For the Mg intercalated bilayer borophenes, we show the projected EDOS and Fermi surface in Fig. 2. From B_2MgB_2 to B_5MgB_5 , the amplitude of the p_z orbitals is fairly small, while there are great changes in the amplitude of the in-plane orbitals in the -4 to 4 eV energy range. The in-plane part of the N_F of B_5MgB_5 , which changes a little near the Fermi level, accounts for only 12% of total N_F . Therefore, the Fermi contour of B_5MgB_5 almost all consists of p_z -derived pockets. The Fermi contour of B_2MgB_2 consists of a double ring pocket and a double star pocket centered at the Γ point derived from the in-plane orbitals, and the six arms of the double star extended along the six Γ -M directions. The Fermi contour of B_2MgB_2 also includes a big ring pocket centered at the Γ point and a small ring pocket centered at the K point derived from the p_z orbitals. For B_3MgB_3 , the Fermi

contour consists of a rectangular pocket centered at Y (0, 0.5) derived from the in-plane orbitals, and three p_z -derived ellipsoidal pockets centered at X (0.5, 0), S (0.5, 0.5), and Y, respectively. The Fermi contour of B_4MgB_4 shows two p_z -derived dumbbell-shaped pockets centered at Γ with some borders paralleled to the H-H' line, whose midpoint is Y (0, 0.5).

The phonon dispersions with phonon linewidth γ_{qp} , Eliashberg function $\alpha^2F(\omega)$, and $\lambda(\omega)$ are shown in Fig. 3. Our calculations with LDA norm-conserving pseudopotentials show the dynamical stability of these sandwich structures without imaginary phonon frequencies in the Brillouin zone. The B_3MgB_3 -kagome shows the dynamical stability with PBE norm-conserving pseudopotentials, which is consistent with the result of ref. 51. The imaginary phonon frequency of the transverse branch near the Γ point was found in the simulations of borophenes,^{33,35} germanene² and other 2D materials,^{59,60} where the emergence of imaginary frequencies is due to the numerical difficulties in accurate calculation rather than a sign of structural transition.⁵⁹ Imaginary phonon frequencies of the acoustical branch also occur near the Γ point in all these sandwich structures shown in Fig. 1(a) with PBE norm-conserving pseudopotentials. Fortunately, these imaginary frequencies have almost no influence on our EPC results. The λ and T_c are found to be almost the same under both PBE and LDA functionals.

As shown in Fig. 3, the vibration modes in the 400 – 800 cm^{-1} frequency range induce the main EPC in B_2MgB_2 , while those of 100 – 400 cm^{-1} induce the main EPC in B_3MgB_3 and B_4MgB_4 . For B_5MgB_5 , the phonon linewidths of the vibration modes in the 100 – 800 cm^{-1} frequency range are fairly small, leading to a small λ and the disappearance of superconductivity. Fig. 4 shows the EPC distribution in the Brillouin zones of these Mg intercalated borophenes. For B_2MgB_2 and B_3MgB_3 , the region with the largest EPC is around Γ and Y, respectively, which is consistent with the phonon linewidth shown in Fig. 3. For B_4MgB_4 , the point with the

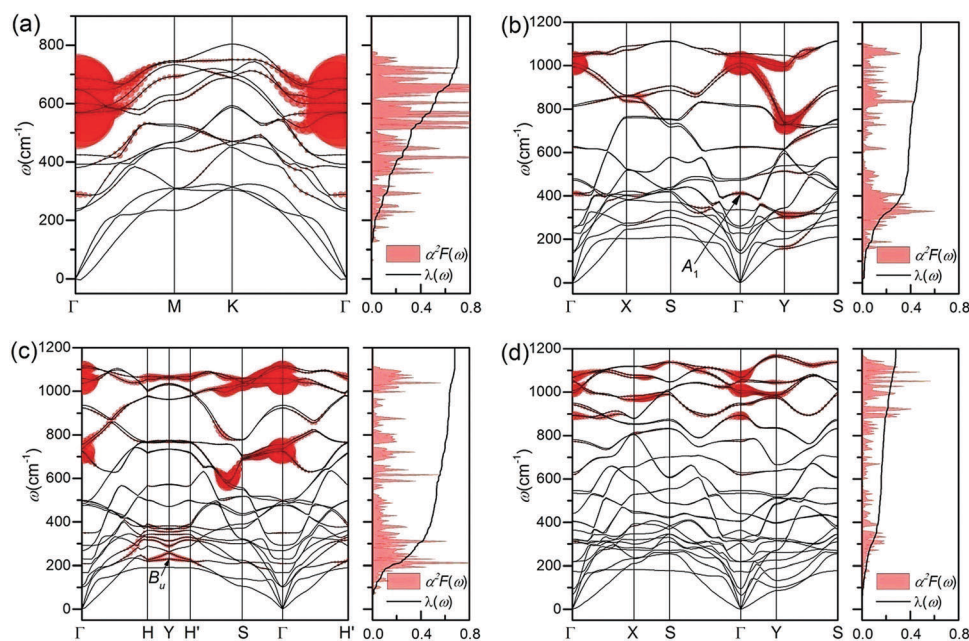


Fig. 3 Phonon dispersion with phonon linewidth γ_{qp} and Eliashberg function $\alpha^2F(\omega)$ with $\lambda(\omega)$ for (a) B_2MgB_2 , (b) B_3MgB_3 , (c) B_4MgB_4 , and (d) B_5MgB_5 .

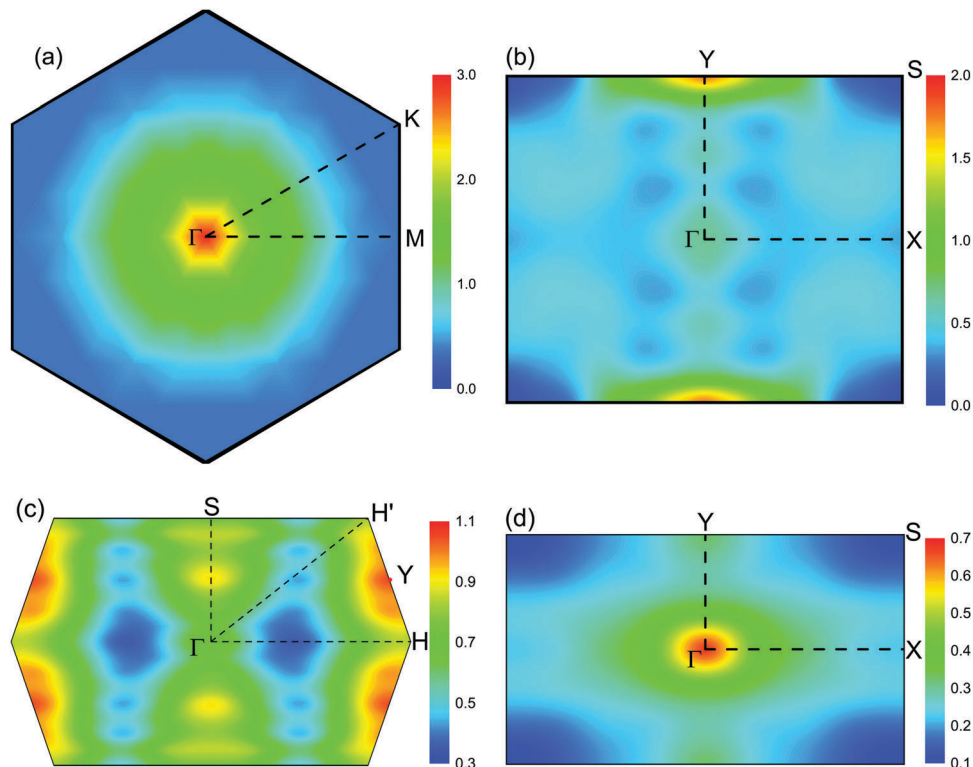


Fig. 4 EPC distributions in the Brillouin zones of (a) B_2MgB_2 , (b) B_3MgB_3 , (c) B_4MgB_4 , and (d) B_5MgB_5 .

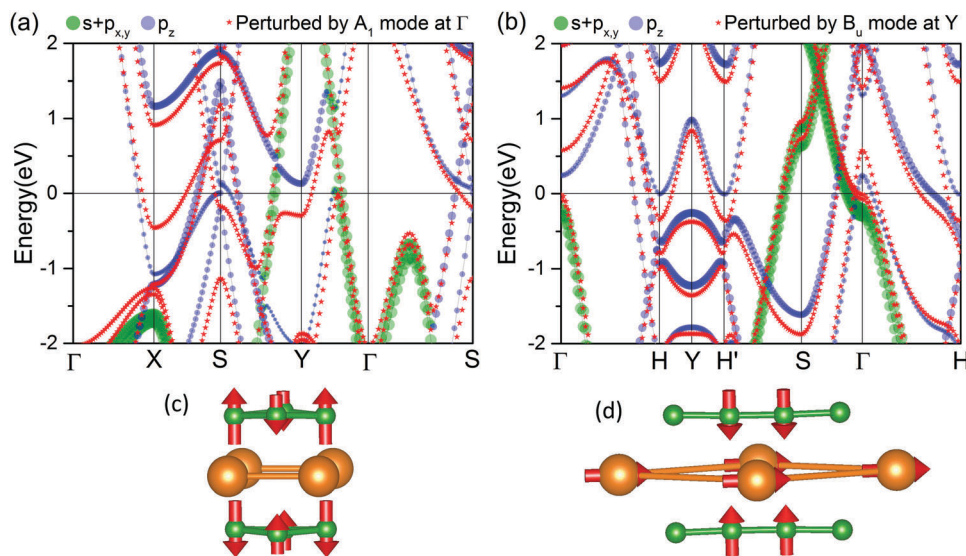


Fig. 5 Orbital-resolved and phonon-perturbed band structures of (a) B_3MgB_3 and (b) B_4MgB_4 , and the corresponding vibrational patterns of (c) B_3MgB_3 and (d) B_4MgB_4 . The sizes of green and blue circles in the band structures represent the weights of the $s + p_x + p_y$ and p_z orbitals of the Mg intercalated bilayer borophenes in the given Kohn–Sham state. The red dots denote the band structures perturbed by phonon modes. The red arrows and their lengths indicate the directions and amplitudes of the corresponding vibrational modes.

largest EPC is Y, and the region with large EPC is along the H–H' line, in which the phonon linewidth is fairly great in the $200\text{--}400\text{ cm}^{-1}$ low frequency range and the $1000\text{--}1100\text{ cm}^{-1}$ high frequency range. For B_5MgB_5 , the region around the Γ point contributes to the major EPC, whose strength is far less than those of B_2MgB_2 , B_3MgB_3 , and B_4MgB_4 .

The EPC in B_xMgB_x is induced by the multiple vibration modes. Fig. 5(a) shows the orbital-resolved band structures of B_3MgB_3 and the band structure perturbed by the A_1 vibrational pattern at Γ (see Fig. 3(b) and 5(c)). This A_1 mode, in which the B atoms vibrate vertically and the Mg atoms remain silent, greatly affects the p_z orbitals near the Fermi level. Fig. 5(b)

shows the orbital-resolved band structures of B_4MgB_4 and the band structure perturbed by the B_u vibrational pattern at Y (see Fig. 3(c) and 5(d)). This B_u mode, in which half of the B atoms vibrate vertically and the Mg atoms vibrate horizontally, greatly affects the p_z orbitals along the H-H' line and the in-plane orbitals along the Γ -S line at the Fermi level.

Conclusion

In summary, we have studied the electronic structure and EPC in Mg intercalated bilayer borophenes, and their corresponding bulk structures. We predict that B_2MgB_2 and B_4MgB_4 should exhibit phonon-mediated superconductivity with a relatively high T_c and B_4MgB_4 would be more practical due to its better stability, indicating the possible superconductivity in the low-dimensional Mg-B system. The Mg intercalation will modulate the EDOS of the in-plane orbitals at the Fermi level, which is dominant at the superconducting T_c in Mg intercalated bilayer borophenes. These findings pave the way for the superconducting applications of two-dimensional Mg-B materials.

Conflicts of interest

There are no conflicts to declare.

Acknowledgements

This work was supported by the NSFC (Grant No. 11474100, 11574088 and 11704322), Guangdong Natural Science Funds for Distinguished Young Scholars (Grant No. 2014A030306024), Guangdong Natural Science Funds for the Doctoral Program (Grant No. 2017A030310086), Fundamental Research Funds for the Central Universities (2017MS119) and Shandong Natural Science Funds for the Doctoral Program (ZR2017BA017). The computer times at the National Supercomputing Center in Guangzhou (NSCCGZ) are gratefully acknowledged.

References

- 1 K. S. Novoselov, A. K. Geim, S. V. Morozov, D. Jiang, Y. Zhang, S. V. Dubonos, I. V. Grigorieva and A. A. Firsov, *Science*, 2004, **306**, 666–669.
- 2 S. Cahangirov, M. Topsakal, E. Aktürk, H. Şahin and S. Ciraci, *Phys. Rev. Lett.*, 2009, **102**, 236804.
- 3 P. Vogt, P. De Padova, C. Quaresima, J. Avila, E. Frantzeskakis, M. C. Asensio, A. Resta, B. Ealet and G. Le Lay, *Phys. Rev. Lett.*, 2012, **108**, 155501.
- 4 G. R. Bhimanapati, Z. Lin, V. Meunier, Y. Jung, J. Cha, S. Das, D. Xiao, Y. Son, M. S. Strano, V. R. Cooper, L. Liang, S. G. Louie, E. Ringe, W. Zhou, S. S. Kim, R. R. Naik, B. G. Sumpter, H. Terrones, F. Xia, Y. Wang, J. Zhu, D. Akinwande, N. Alem, J. A. Schuller, R. E. Schaak, M. Terrones and J. A. Robinson, *ACS Nano*, 2015, **9**, 11509–11539.
- 5 S. Das, M. Demarteau and A. Roelofs, *ACS Nano*, 2014, **8**, 11730–11738.
- 6 G. Yanfeng, W. Wenhui, Y. Fan and Y. Yugui, *New J. Phys.*, 2015, **17**, 035008.
- 7 M. Corso, W. Auwärter, M. Muntwiler, A. Tamai, T. Greber and J. Osterwalder, *Science*, 2004, **303**, 217–220.
- 8 M. Chen, Y.-J. Zhao, J.-H. Liao and X.-B. Yang, *Phys. Rev. B: Condens. Matter Mater. Phys.*, 2012, **86**, 045459.
- 9 E. D. Sandoval, S. Hajinazar and A. N. Kolmogorov, *Phys. Rev. B*, 2016, **94**, 094105.
- 10 E. S. Penev, S. Bhowmick, A. Sadrzadeh and B. I. Yakobson, *Nano Lett.*, 2012, **12**, 2441–2445.
- 11 X. J. Wu, J. Dai, Y. Zhao, Z. W. Zhuo, J. L. Yang and X. C. Zeng, *ACS Nano*, 2012, **6**, 7443–7453.
- 12 X. Yu, L. Li, X.-W. Xu and C.-C. Tang, *J. Phys. Chem. C*, 2012, **116**, 20075–20079.
- 13 H. G. Lu, Y. W. Mu, H. Bai, Q. Chen and S. D. Li, *J. Chem. Phys.*, 2013, **138**, 024701.
- 14 H. Tang and S. Ismail-Beigi, *Phys. Rev. Lett.*, 2007, **99**, 115501.
- 15 X. Yang, Y. Ding and J. Ni, *Phys. Rev. B: Condens. Matter Mater. Phys.*, 2008, **77**, 041402.
- 16 A. J. Mannix, X. F. Zhou, B. Kiraly, J. D. Wood, D. Alducin, B. D. Myers, X. L. Liu, B. L. Fisher, U. Santiago, J. R. Guest, M. J. Yacaman, A. Ponce, A. R. Oganov, M. C. Hersam and N. P. Guisinger, *Science*, 2015, **350**, 1513–1516.
- 17 B. Feng, J. Zhang, Q. Zhong, W. Li, S. Li, H. Li, P. Cheng, S. Meng, L. Chen and K. Wu, *Nat. Chem.*, 2016, **8**, 564–569.
- 18 Y. Y. Liu, E. S. Penev and B. I. Yakobson, *Angew. Chem.*, 2013, **52**, 3156–3159.
- 19 Z. Zhang, Y. Yang, G. Gao and B. I. Yakobson, *Angew. Chem.*, 2015, **127**, 13214–13218.
- 20 S. G. Xu, Y. J. Zhao, J. H. Liao, X. B. Yang and H. Xu, *Nano Res.*, 2016, **9**, 2616–2622.
- 21 B. Feng, J. Zhang, R.-Y. Liu, T. Iimori, C. Lian, H. Li, L. Chen, K. Wu, S. Meng, F. Komori and I. Matsuda, *Phys. Rev. B*, 2016, **94**, 041408.
- 22 H. Shu, F. Li, P. Liang and X. Chen, *Nanoscale*, 2016, **8**, 16284–16291.
- 23 L. Shi, C. Ling, Y. Ouyang and J. Wang, *Nanoscale*, 2017, **9**, 533–537.
- 24 X. Zhang, J. Hu, Y. Cheng, H. Y. Yang, Y. Yao and S. A. Yang, *Nanoscale*, 2016, **8**, 15340–15347.
- 25 L. Zhang, P. Liang, H.-b. Shu, X.-l. Man, F. Li, J. Huang, Q.-m. Dong and D.-l. Chao, *J. Phys. Chem. C*, 2017, **121**, 15549–15555.
- 26 H. R. Jiang, Z. Lu, M. C. Wu, F. Ciucci and T. S. Zhao, *Nano Energy*, 2016, **23**, 97–104.
- 27 H. Zhang, Y. Xie, Z. Zhang, C. Zhong, Y. Li, Z. Chen and Y. Chen, *J. Phys. Chem. Lett.*, 2017, **8**, 1707–1713.
- 28 V. V. Kulish, *Phys. Chem. Chem. Phys.*, 2017, **19**, 11273–11281.
- 29 B. Onat, L. Hallioglu, S. Ipek and E. Durgun, *J. Phys. Chem. C*, 2017, **121**, 4583–4592.
- 30 X. Sun, X. Liu, J. Yin, J. Yu, Y. Li, Y. Hang, X. Zhou, M. Yu, J. Li, G. Tai and W. Guo, *Adv. Funct. Mater.*, 2017, **27**, 1603300.
- 31 J. E. Padilha, R. H. Miwa and A. Fazzio, *Phys. Chem. Chem. Phys.*, 2016, **18**, 25491–25496.

- 32 L.-C. Xu, A. Du and L. Kou, *Phys. Chem. Chem. Phys.*, 2016, **18**, 27284–27289.
- 33 E. S. Penev, A. Kutana and B. I. Yakobson, *Nano Lett.*, 2016, **16**, 2522–2526.
- 34 Y. Zhao, S. Zeng and J. Ni, *Appl. Phys. Lett.*, 2016, **108**, 242601.
- 35 M. Gao, Q.-Z. Li, X.-W. Yan and J. Wang, *Phys. Rev. B*, 2017, **95**, 024505.
- 36 R. C. Xiao, D. F. Shao, W. J. Lu, H. Y. Lv, J. Y. Li and Y. P. Sun, *Appl. Phys. Lett.*, 2016, **109**, 122604.
- 37 C. Cheng, J. T. Sun, H. Liu, H. X. Fu, J. Zhang, X. R. Chen and S. Meng, *2D Mater.*, 2017, **4**, 025032.
- 38 C. Wu, H. Wang, J. Zhang, G. Gou, B. Pan and J. Li, *ACS Appl. Mater. Interfaces*, 2016, **8**, 2526–2532.
- 39 B. Uchoa and A. H. Castro Neto, *Phys. Rev. Lett.*, 2007, **98**, 146801.
- 40 G. Profeta, M. Calandra and F. Mauri, *Nat. Phys.*, 2012, **8**, 131–134.
- 41 N. Emery, C. Hérold, M. d'Astuto, V. Garcia, C. Bellin, J. F. Maréché, P. Lagrange and G. Louprias, *Phys. Rev. Lett.*, 2005, **95**, 087003.
- 42 T. E. Weller, M. Ellerby, S. S. Saxena, R. P. Smith and N. T. Skipper, *Nat. Phys.*, 2005, **1**, 39–41.
- 43 S. Ichinokura, K. Sugawara, A. Takayama, T. Takahashi and S. Hasegawa, *ACS Nano*, 2016, **10**, 2761–2765.
- 44 Y. Zhao, S. Zeng and J. Ni, *Phys. Rev. B*, 2016, **93**, 014502.
- 45 J. Nagamatsu, N. Nakagawa, T. Muranaka, Y. Zenitani and J. Akimitsu, *Nature*, 2001, **410**, 63–64.
- 46 J. M. An and W. E. Pickett, *Phys. Rev. Lett.*, 2001, **86**, 4366–4369.
- 47 Y. Kong, O. V. Dolgov, O. Jepsen and O. K. Andersen, *Phys. Rev. B: Condens. Matter Mater. Phys.*, 2001, **64**, 020501.
- 48 J. Kortus, I. I. Mazin, K. D. Belashchenko, V. P. Antropov and L. L. Boyer, *Phys. Rev. Lett.*, 2001, **86**, 4656–4659.
- 49 T. Yildirim, O. Gülseren, J. W. Lynn, C. M. Brown, T. J. Udovic, Q. Huang, N. Rogado, K. A. Regan, M. A. Hayward, J. S. Slusky, T. He, M. K. Haas, P. Khalifah, K. Inumaru and R. J. Cava, *Phys. Rev. Lett.*, 2001, **87**, 037001.
- 50 M. M. D. Esfahani, Q. Zhu, H. Dong, A. R. Oganov, S. Wang, M. S. Rakitin and X.-F. Zhou, *Phys. Chem. Chem. Phys.*, 2017, **19**, 14486–14494.
- 51 S.-Y. Xie, X.-B. Li, W. Q. Tian, N.-K. Chen, Y. Wang, S. Zhang and H.-B. Sun, *Phys. Chem. Chem. Phys.*, 2015, **17**, 1093–1098.
- 52 P. Giannozzi, S. Baroni, N. Bonini, M. Calandra, R. Car, C. Cavazzoni, D. Ceresoli, G. L. Chiarotti, M. Cococcioni, I. Dabo, A. Dal Corso, S. de Gironcoli, S. Fabris, G. Fratesi, R. Gebauer, U. Gerstmann, C. Gougoussis, A. Kokalj, M. Lazzeri, L. Martin-Samos, N. Marzari, F. Mauri, R. Mazzarello, S. Paolini, A. Pasquarello, L. Paulatto, C. Sbraccia, S. Scandolo, G. Sclauzero, A. P. Seitsonen, A. Smogunov, P. Umari and R. M. Wentzcovitch, *J. Phys.: Condens. Matter*, 2009, **21**, 395502.
- 53 M. Methfessel and A. T. Paxton, *Phys. Rev. B: Condens. Matter Mater. Phys.*, 1989, **40**, 3616–3621.
- 54 H. J. Monkhorst and J. D. Pack, *Phys. Rev. B: Solid State*, 1976, **13**, 5188–5192.
- 55 P. B. Allen and R. C. Dynes, *Phys. Rev. B: Solid State*, 1975, **12**, 905–922.
- 56 S. V. Barabash, V. Blum, S. Müller and A. Zunger, *Phys. Rev. B: Condens. Matter Mater. Phys.*, 2006, **74**, 035108.
- 57 H. J. Choi, D. Roundy, H. Sun, M. L. Cohen and S. G. Louie, *Phys. Rev. B: Condens. Matter Mater. Phys.*, 2002, **66**, 020513.
- 58 J. Bardeen, L. N. Cooper and J. R. Schrieffer, *Phys. Rev.*, 1957, **106**, 162–164.
- 59 H. Şahin, S. Cahangirov, M. Topsakal, E. Bekaroglu, E. Akturk, R. T. Senger and S. Ciraci, *Phys. Rev. B: Condens. Matter Mater. Phys.*, 2009, **80**, 155453.
- 60 C. Kamal and M. Ezawa, *Phys. Rev. B: Condens. Matter Mater. Phys.*, 2015, **91**, 085423.